Applied Geochemistry 126 (2021) 104864

Contents lists available at ScienceDirect

Applied Geochemistry

journal homepage: http://www.elsevier.com/locate/apgeochem

Complexation of Nd(III)/Cm(III) with gluconate in alkaline NaCl and $CaCl_2$ solutions: Solubility, TRLFS and DFT studies

Henar Rojo [a,*,1], Xavier Gaona [b,**], Thomas Rabung [b], Robert Polly [b], Miguel García-Gutiérrez [a], Tiziana Missana [a], Marcus Altmaier [b]

[a] Department of Environment, CIEMAT, Madrid, Spain
[b] Institute for Nuclear Waste Disposal, Karlsruhe Institute of Technology, Karlsruhe, Germany

ARTICLE INFO

Editorial handling by Dr. Z Zimeng Wang

Keywords:
Neodymium(III)
Curium(III)
Gluconate
Calcium
Solubility
TRLFS
DFT

ABSTRACT

The effect of gluconate on the solubility and aqueous speciation of An(III) and Ln(III) was studied using a combination of Nd(III) solubility experiments, Cm(III) time-resolved laser fluorescence spectroscopy (TRLFS) and density functional theory (DFT) calculations.

Solubility experiments were performed under an Ar-atmosphere using a well-defined $Nd(OH)_3$(s) solid phase equilibrated in NaCl (0.1–5.0 M) and $CaCl_2$ (0.1–3.5 M) solutions with $9 \leq pH_c \leq 13$ and 10^{-6} M $\leq [GLU]_{tot} \leq 10^{-2}$ M. The solubility of $Nd(OH)_3$(s) remains mostly unaffected in NaCl solutions with $[GLU]_{tot} = 10^{-3}$ M, whereas a clear increase in solubility is observed in dilute $CaCl_2$ solutions with the same $[GLU]_{tot}$ and $pH_c \geq 11$. In concentrated $CaCl_2$ solutions, gluconate does not affect the solubility of Nd(III) due to the competition with Ca–GLU complexes.

Cm(III) TRLFS spectra collected in NaCl solutions with $pH_c \approx 12$ confirm the formation of weak Cm(III)–GLU complexes. The very strong red shift observed in dilute $CaCl_2$ solutions in connection with high fluorescence intensities supports the formation of ternary Ca–Cm(III)–GLU complexes. The speciation of Cm(III) in 3.5 M $CaCl_2$ solutions is mostly dominated by the complex $Ca_3[Cm(OH)_6]^{3+}$, although the formation of ternary Ca–Cm(III)–GLU species is hinted at high gluconate concentrations. DFT calculations provide additional support to the formation of stable ternary Ca–Cm(III)–GLU aqueous complexes.

This work provides key information to understand the chemical speciation and relevant equilibrium processes of An(III) and Ln(III) in the presence of gluconate under conditions relevant for nuclear waste disposal.

1. Introduction

The use of cementitious materials is considered for the solidification/stabilization of the waste forms, as backfill material and for construction purposes in most of the current repository concepts for the disposal of low and intermediate level radioactive waste (L/ILW). The equilibration of the main mineral phases of these materials (Na_2O/K_2O, $Ca(OH)_2$, calcium silicate hydrates (C–S–H phases)) with groundwater imposes hyperalkaline pH conditions (10–13.3) over very long time scales. Relatively high calcium concentrations (1–20 mM) are also present in solution due to the equilibrium with portlandite ($Ca(OH)_2$(s)) and C–S–H phases with Ca:Si ratio greater than 1 (Berner, 1992; Kulik, 2011). In the context of waste disposal in rock salt formations, the corrosion of cementitious waste forms has been reported to potentially generate $CaCl_2$-rich brines (up to 4 M) in combination with very high pH values ($pH_m \approx 12$, with $pH_m = -\log [H^+]$ in molal units) (Bube et al., 2013). Intermediate ionic strength conditions ($I = 2$–3 M) are also found in Cretaceous argillites in Northern Germany (Brewitz, 1980), whose pore water is mostly dominated by NaCl and $CaCl_2$.

Under the reducing conditions expected in underground repositories for the disposal of radioactive waste, key actinides will be found in the +III and +IV oxidation state. These oxidation states are characterized by a tendency towards very high sorption retention and low solubility, especially under hyperalkaline conditions, where the formation of the sparingly soluble (oxy-)hydroxide phases $An(OH)_3$(am) and AnO_2(am, hyd) leads to $[An]_{aq}$ below 10^{-8} M (Altmaier et al., 2013; Grenthe et al.,

* Corresponding author.
** Corresponding author.
E-mail addresses: henar.rojo@mavt.ethz.ch (H. Rojo), xavier.gaona@kit.edu (X. Gaona).
[1] Current address: Optical Materials Engineering Laboratory (OMEL), ETH Zurich, CNB G 130.1; Universitätstrasse 6, CH-8092 Zürich.

https://doi.org/10.1016/j.apgeochem.2020.104864
Received 5 October 2020; Received in revised form 7 December 2020; Accepted 17 December 2020
Available online 27 December 2020

2020; Guillaumont et al., 2003; Neck et al., 2009; Neck and Kim, 2001). Radionuclide sorption and solubility in cementitious and saline systems can be affected by the presence of organic ligands. Poly–hydroxycarboxylic acids such as gluconic acid ($C_6H_{12}O_7$/HGLU) and isosaccharinic acid ($C_6H_{12}O_6$/HISA) are expected in repositories for L/ILW as additive in cementitious materials and as main cellulosic degradation product, respectively (Fig. 1). These ligands are generically quoted as GLU and ISA in the following.

Under hyperalkaline conditions and in the presence of hard Lewis acids, alcohol groups of gluconic and isosaccharinic acids are prone to deprotonate and contribute to the formation of very stable chelate complexes (Bechtold et al., 2002; Giroux et al., 2000; Moreton et al., 2000; Motekaitis and Martell, 1984; Pallagi et al., 2013). Although several studies have confirmed the strong complexation of these ligands with An(III) and An(IV) (Allard, 2005; Allard and Ekberg, 2006; Colàs, 2014; Colàs et al., 2011, 2013a, 2013b; Gaona et al., 2008; Moreton, 1993, 2000; Rai et al., 1998, 2003, 2009; Rojo et al., 2013; Tasi et al., 2018a, 2018b; Tits et al., 2005; Vercammen, 2000; Vercammen et al., 1999, 2001; Zhang et al., 2007), relevant discrepancies and uncertainties affecting the stoichiometry and stability of these complexes remain. The formation of ternary species of the type Ca–An–GLU/ISA has been reported for An(IV), but no evidence on the formation of analogous species with An(III) or Ln(III) is available so far in the literature.

For experimental studies assessing the formation of actinide complexes with gluconate in the presence of calcium, an accurate knowledge of the binary system Ca–GLU is also needed. The analogy with the system Ca–ISA was the main source of thermodynamic data for the gluconate counterpart until recently, when a comprehensive study by Pallagi and co-workers was published (Pallagi et al., 2014). Based on a combination of ^{13}C–NMR, potentiometry, conductometry and freezing point techniques, the authors derived chemical and thermodynamic models for the system Ca^{2+}–GLU^- in alkaline to hyperalkaline conditions, which included the very stable neutral species CaOHGLU(aq) (or $CaGLU_{-H}$(aq), where "–H" corresponds to the deprotonation of an alcohol group of gluconate), $Ca_2(OH)_3GLU$(aq) (or Ca_2GLU_{-3H}(aq)) and $Ca_3(OH)_4(GLU)_2$(aq) (or $Ca_3(GLU_{-2H})_2$(aq)). From these species, only CaOHGLU (aq) was previously included in the reported chemical and thermodynamic models. The thermodynamics and coordination chemistry of the system Ca–GLU–H_2O have been recently reviewed by Kutus and co-workers (Kutus et al., 2020). Note that the use of inaccurate chemical and thermodynamic models for the binary system Ca–GLU can expectedly hinder the quality of the accordingly derived thermodynamic models for the ternary systems Ca–An(III)/An(IV)–GLU.

In this context, this study aims at assessing the solubility and aqueous speciation of Nd(III)/Cm(III) in alkaline solutions in the presence of gluconate, with special emphasis in evaluating the role of Ca and the formation of ternary complexes Ca–Ln(III)/An(III)–GLU. This work combines systematic solubility experiments conducted with $Nd(OH)_3$(s) in alkaline NaCl and $CaCl_2$ solutions in the presence of gluconate, with Cm(III)–TRLFS spectroscopic measurements conducted under analogous experimental conditions. Density functional theory (DFT) calculations are also used to gain further insight on the Ln(III)/An(III) speciation in the presence of gluconate and calcium.

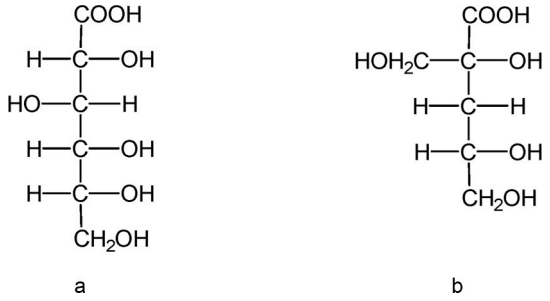

Fig. 1. Chemical formula of (a) D-gluconic acid ($C_6H_{12}O_7$, HGLU) and (b) a-Isosaccharinic acid ($C_6H_{12}O_6$, HISA).

2. Materials and methods

2.1. Chemicals

All solutions and samples were prepared, stored, and handled inside an inert gas (Ar) glovebox at $t = (22 \pm 2)$ °C. All solutions were prepared with ultrapure water purified with a Milli-Q-academic (Millipore) apparatus and purged with Ar before use. NaCl (p.a.), NaOH (Titrisol®), HCl (Titrisol®), $CaCl_2{\cdot}2H_2O$ (p.a.), $Ca(OH)_2$ (p.a.) and $NaC_6H_{11}O_7$ (NaGLU, p.a., 99%) were purchased from Merck. $CaC_{12}H_{24}O_{15}$ ($Ca(GLU)_2{\cdot}H_2O$, 97%) was obtained from AppliChem.

Solubility experiments were conducted with $Nd(OH)_3$(s) prepared by hydration of Nd_2O_3(cr) (Merck, 99% – see section 2.3). The long-lived curium isotope Cm–248 ($t_{1/2} = 3.4 \times 10^5$ years) was used for TRLFS experiments. The original stock solution (1×10^{-5} M Cm(III) in 0.1 M $HClO_4$) had an isotopic composition of 97.3% Cm–248, 2.6% Cm–246, 0.04% Cm–245, 0.02% Cm–247 and 0.009% Cm–244.

2.2. Measurements of pH

A combination glass pH electrode (type ROSS, Orion), freshly calibrated against dilute standard pH buffers (pH 8–13, Merck), was used to determine the molar H^+ concentration, $[H^+]$ (with $pH_c = -\log [H^+]$). In salt solutions of ionic strength $I \geq 0.1$ M, the measured pH value (pH_{exp}) is an operational apparent value related to $[H^+]$ by $pH_c = pH_{exp} + A_c$, where A_c is given as a function of the NaCl and $CaCl_2$ concentration (Altmaier et al., 2003, 2008). This approach is equivalent to calibrating the electrode *vs.* standard samples with fixed proton concentration at constant background electrolyte concentrations and relates the potential measured in the samples to the proton concentrations on a molar scale. In $CaCl_2$ solutions, the highest pH_c (pH_{max}) is fixed by the precipitation of $Ca(OH)_2$(s) (or mixed Ca–OH–Cl compounds like $Ca_4(OH)_6Cl_2{\cdot}13H_2O$ (s) at Ca concentrations above ≈ 2 m), which buffer pH_c at ≈ 12.

2.3. Nd(III) solid phase preparation and characterization. Solubility measurements

The solid phase $Nd(OH)_3$(s) used for solubility experiments was prepared under an Ar atmosphere by hydration of crystalline Nd_2O_3(cr) in Milli-Q water during 3 months. The complete transformation of the oxide into hydroxide phase was confirmed by X-ray diffraction (XRD). Undersaturation solubility experiments were prepared with 5–10 mg of $Nd(OH)_3$(s) in contact with 20 ml of solution per individual batch sample. Experiments were performed in 0.1 and 5.0 M NaCl–NaOH solutions with $9 \leq pH_c \leq 13$, and in 0.25 and 3.5 M $CaCl_2$ solutions with $9 \leq pH_c \leq 12$. Additional experimental series were prepared in 0.1 and 0.25 M $CaCl_2$ solutions with pH_c = constant ≈12 and $10^{-6} \leq [GLU] \leq 10^{-2}$ M. Solution parameters pH_c and [Nd] were monitored for up to 400 days. The concentration of Nd in the aqueous phase was quantified by inductively coupled plasma mass spectrometry (ICP–MS, ELAN 6100, PerkinElmer) after phase separation by 10 kD ultrafiltration (pore size ≈ 2–3 nm, Nanosep®, Pall Life Sciences). The limit of detection (LOD) of the ICP–MS measurements ranged between $2{\cdot}10^{-10}$ and $1{\cdot}10^{-8}$ M, depending on the dilution factor required for a given salt concentration. The concentration of gluconate in the supernatant of selected solubility samples was quantified as total organic content using a Shimadzu TOC5000 analyzer (LOD ≈ 0.1 ppm C; ≈ 1×10^{-5} M GLU considering the corresponding dilution factor).

Original unhydrated Nd_2O_3(cr), $Nd(OH)_3$(s) obtained by hydration of the anhydrous oxide, as well as selected solid phases collected after termination of the solubility experiments in the presence of GLU, were characterized by XRD with a Bruker D8 diffractometer equipped with a

Si(Li) solid state detector. Solid phases recovered from solubility experiments were washed five times with ethanol to remove the salt content adhering to the solid before the characterization by XRD. An air-tight sample holder (Bruker) was used for the measurements. XRD data were collected within $5° \leq 2\theta \leq 60°$, using a step size of 0.02° and accumulation times of 60 s per single step.

2.4. Cm(III) TRLFS

All TRLFS samples were prepared and stored at $t = (22 \pm 2)$ °C in a glovebox under an Ar-atmosphere. TRLFS measurements were performed with $\approx 10^{-7}$ M Cm(III) per sample, in solutions at $pH_c \approx$ constant ≈ 12 containing: (i) 0.1 M NaCl; (ii) 0.1 M NaCl + 0.001 M $CaCl_2$; (iii) 0.1 M NaCl + 0.01 M $CaCl_2$; (iv) 0.1 M $CaCl_2$; (v) 0.25 M $CaCl_2$; and (vi) 3.5 M $CaCl_2$. The initial concentration of GLU in all samples (10^{-6} M) was increased to 3×10^{-3} M by step-wise additions of NaGLU–NaCl or $Ca(GLU)_2$–$CaCl_2$ solutions of the same ionic strength and composition as the sample matrix solution. After each addition, samples were equilibrated for 1 day before the next measurement. The sorption of the Cm (III)–GLU complexes on the cuvette surface was tested for $t \leq 5$ days, resulting in no significant loss of the fluorescence intensity and hence confirming negligible sorption losses when using this experimental setup.

TRLFS measurements were performed using a pulsed Nd:YAG pumped dye laser system (Continuum, Powerlite 9030, ND 6000) at a repetition rate of 10 Hz and a maximum laser energy of 3.5 mJ. To filter out light scattering and background fluorescence, the emission spectra were recorded in the range of 590–630 nm and 1 μs after the exciting laser pulse in a time window of 1 ms and at $\lambda_{exc} = 396.6$ nm (laser dye: Exalite 398). The fluorescence emission was detected by an optical multi-channel analyzer consisting of a polychromator (Chromex 250 is) with 300, 600 and 1200 lines/nm grating. The latter one was used for measuring the fluorescence spectra.

2.5. Theoretical methods

The structures of selected ternary Ca–Nd(III)–GLU complexes were investigated by means of density functional theory (DFT) calculations (Hohenberg and Kohn, 1964; Kohn and Sham, 1965). DFT calculations were performed using TURBOMOLE (version 7.0, 2015) (Deglmann et al., 2004; Eichkorn et al., 1995, 1997; Furche et al., 2014; Schäfer et al., 1992; Treutler and Ahlrichs, 1995; Von Arnim and Ahlrichs, 1999) with the BP86 functional (Ahlrichs et al., 2000) and the def2-SVP basis set (Schäfer et al., 1992) on C, O, Ca and H. The use of 4f-in core pseudo potentials (PP) for Nd(III) (Dolg et al., 1989, 1993) allowed to circumvent several problems arising with DFT calculations involving lanthanides: (i) difficulties due to open shells can be avoided, (ii) multi reference effects do not occur and (iii) the number of electrons and thus the computer time is greatly reduced. This leads to a theoretical task suited for DFT, and avoids complex and computationally very demanding multi reference *ab initio* methods.

For a more realistic description of the Ca–Nd(III)–GLU systems investigated, several water molecules were explicitly considered in the calculations. A second step in the calculations included the aqueous media approximated with the conductor-like screening model (COSMO) (Klamt, 1995; Klamt and Schüürmann, 1993). Considering the first water shell explicitly and dealing with the additional solvation effects by means of COSMO provide a rather realistic model to investigate species in aqueous solution. This methodology was already tested and verified in earlier studies combining theoretical and experimental methods (Tasi et al., 2018a, 2018b).

3. Results and discussion

3.1. Solubility of Nd(III) in NaCl and $CaCl_2$ solutions in the presence of GLU

Fig. 2 shows the solubility data of $Nd(OH)_3$(s) determined at $9 \leq pH_c \leq 13$, in solutions containing $[GLU]_{tot}$ = constant = 10^{-3} M and (a) 0.1 M NaCl, (b) 5.0 M NaCl, (c) 0.25 M $CaCl_2$, and (d) 3.5 M $CaCl_2$. Fig. 2a–d include also experimental solubility data and model calculations reported by Neck et al. (2009) for analogous boundary conditions but absence of gluconate. The same method was used by Neck and co-workers and in this work for the synthesis of $Nd(OH)_3$(s), and thus the solubility data reported by the former are considered an appropriate baseline to assess the impact of gluconate on the solubility.

Gluconate (at $[GLU]_{tot} = 10^{-3}$ M) has no clear effect on the solubility of Nd(III) in the investigated NaCl solutions (Fig. 2a and b). The slight, minor increase of solubility hinted in dilute NaCl solutions at $pH_c > 12$ (Fig. 2a), is not confirmed by solubility data in 5.0 M NaCl–NaOH systems with $pH_c \leq 14.0$. These results are in disagreement with a previous sorption study investigating the Eu(III)/Am(III)–GLU system (Tits et al., 2005), which reported the formation of binary complexes with gluconate at $[GLU]_{tot} \geq 10^{-7}$ M. In this previous study, sorption experiments were performed with calcite in artificial cement pore water (ACW), *i.e.* at pH = 13.3 and containing 0.18 M KOH, 0.114 M NaOH and $1.6 \cdot 10^{-3}$ M $Ca(OH)_2$. The participation of Ca on the complex formation was disregarded in Tits et al. (2005) based on the analogy with previous (sorption) experiments with the Eu(III)–ISA system (Vercammen et al., 2001).

In contrast to the solubility data in NaCl solutions, a significant increase in the concentration of Nd(III) compared to gluconate-free systems is observed in 0.25 M $CaCl_2$ solutions with $[GLU]_{tot} = 10^{-3}$ M and $pH_c \geq 11$ (Fig. 2c). The solubility increases with a steep slope (log [Nd] *vs.* pH_c) of +3/+4, indicating that 3 to 4 protons are released in the equilibrium reaction controlling the solubility of Nd(III) in this pH_c-region. This observation, in combination with the limited impact of gluconate in the solubility of Nd(III) in Ca-free systems, provides indirect evidence on the formation of ternary complexes Ca–Nd(III)–GLU in 0.25 M $CaCl_2$ solutions. A clear increase in the solubility of Nd(III) is also observed in 3.5 M $CaCl_2$ systems with $[GLU]_{tot} = 10^{-3}$ M and $pH_c \geq 11$. Such observation, however, perfectly matches solubility data in the absence of gluconate as previously reported in the literature (Neck et al., 2009). Neck and co-workers explained the increase in solubility with the formation of ternary Ca–Ln(III)/An(III)–OH complexes in concentrated $CaCl_2$ solutions ($Ca[M(OH)_3]^{2+}$, $Ca_2[M(OH)_4]^{3+}$ and $Ca_3[M(OH)_6]^{3+}$), as also described for a number of M(IV) (with M = Th, Np, Pu, Zr, Tc) (Altmaier et al., 2008, 2009; Fellhauer et al., 2010; Yalçintaş et al., 2016) and Np(V) systems (Fellhauer et al., 2016a, 2016b). These results indicate that, if forming in concentrated $CaCl_2$ solutions, the ternary complexes Ca–Nd(III)–GLU have a minor impact on the solubility of Nd (III). This can be possibly explained by the predominance of binary Ca–GLU complexes that outcompete the complexation with Nd(III).

Fig. 3 shows the solubility of $Nd(OH)_3$(s) in 0.1 M $CaCl_2$ (figure a) and 0.25 M $CaCl_2$ (figure b) solutions with pH_c = constant ≈ 12 and $10^{-6} \leq [GLU]_{tot} \leq 10^{-2}$. Fig. 3 also includes the solubility of Nd(III) in gluconate-free systems calculated using the thermodynamic and SIT activity models reported in Neck et al. (2009). In both systems, a clear enhancement of Nd(III) solubility occurs at $[GLU]_{tot} \geq 10^{-4}$ M. The increase in solubility is significant at $[GLU]_{tot} = 10^{-4}$–10^{-3} M, but somehow constant [Nd(III)] are measured above $[GLU]_{tot} \approx 10^{-3}$ M (coloured red and blue areas in Fig. 3a and b, respectively). The dispersion of the measured Nd(III) concentrations (especially in 0.25 M $CaCl_2$) does not allow a definitive slope analysis of the solubility data. However, a combined evaluation of both datasets (0.1 and 0.25 M $CaCl_2$) suggests a slope of +2 as more plausible option, which would indicate the formation of an aqueous complex with stoichiometry Nd : GLU = 1 : 2. The flattening of the solubility observed at $[GLU]_{tot} > 10^{-3}$

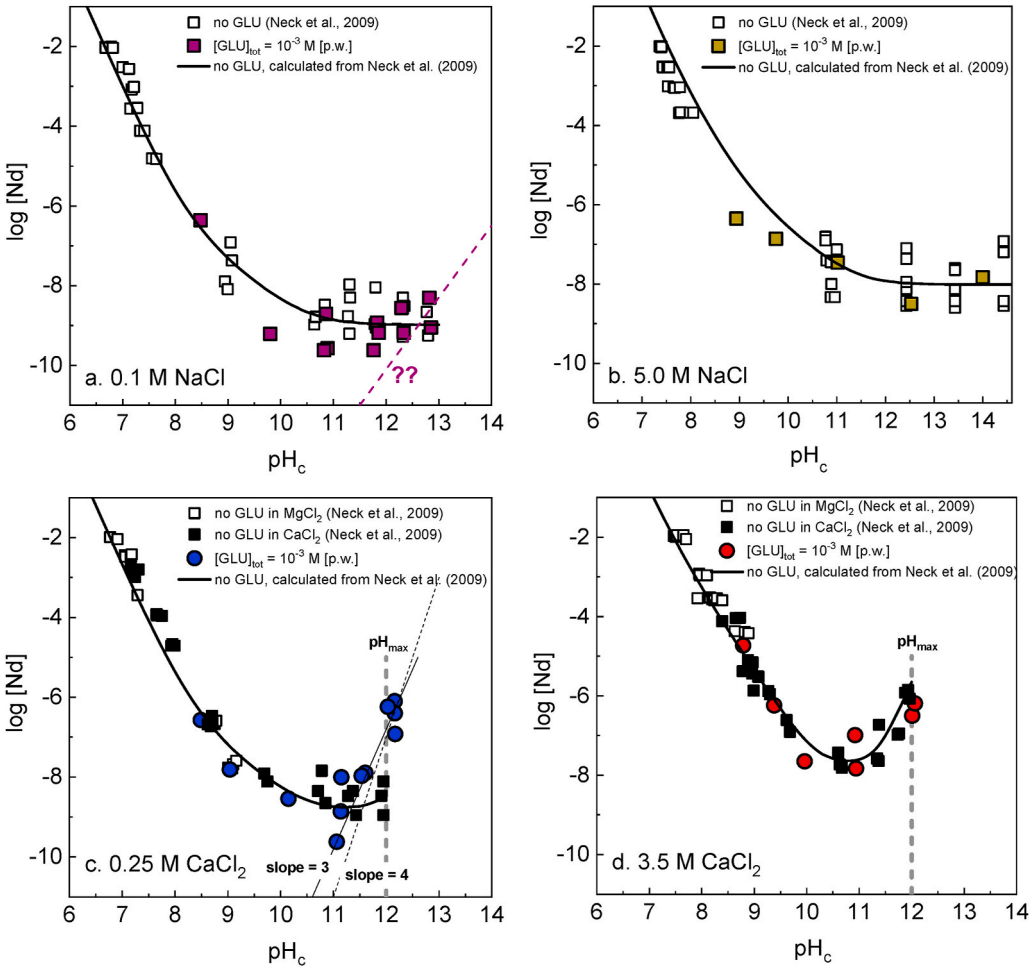

Fig. 2. Solubility of $Nd(OH)_3(s)$ in the presence of $[GLU]_{tot}$ = constant = 10^{-3} M and (a) 0.1 M NaCl; (b) 5.0 M NaCl; (c) 0.25 M $CaCl_2$; (d) 3.5 M $CaCl_2$. Empty symbols in the figures correspond to solubility data determined under analogous conditions but absence of gluconate (Neck et al., 2009). Solid lines represent the solubility of $Nd(OH)_3(s)$ in the absence of gluconate calculated with the thermodynamic and SIT activity models reported in Neck et al. (2009).

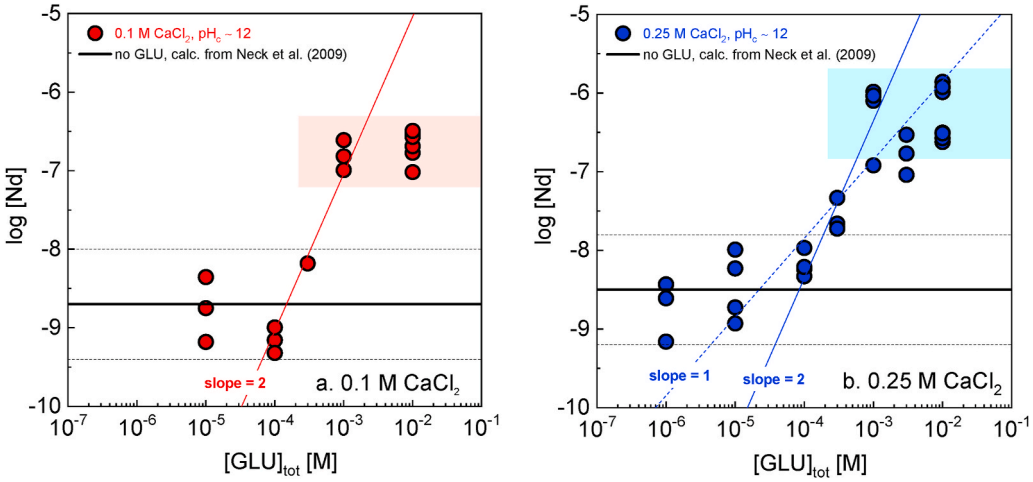

Fig. 3. Solubility of $Nd(OH)_3(s)$ at $pH_c \approx 12$ in the presence of 10^{-6} M $\leq [GLU]_{tot} \leq 10^{-2}$ M and (a) 0.1 M $CaCl_2$; (b) 0.25 M $CaCl_2$. Solid lines represent the solubility of $Nd(OH)_3(s)$ in the absence of gluconate calculated with the thermodynamic and SIT activity models reported in Neck et al. (2009).

M (especially in Fig. 3a) can only be explained by the formation of a new Nd(III) solid phase involving the participation of GLU and (most likely) Ca. A detailed discussion on this hypothesis is provided in Section 3.2.

3.2. Characterization of aqueous and solid phases in selected solubility experiments

The concentration of gluconate in the aqueous phase after attaining equilibrium conditions was quantified by TOC for samples in 0.1 M NaCl

and 0.25 M $CaCl_2$ containing 10^{-4} M ≤ $[GLU]_{tot}$ ≤ 10^{-2} M (Fig. 4). In all cases, no significant changes from the initial concentration of soluble gluconate were observed, thus supporting that practically all of the initial soluble gluconate is remaining in solution (albeit, relative to our measurement capabilities which could not detect minor changes that could result from the precipitation of a secondary phase Ca–Nd(III)-GLU). In a previous solubility study on the system Th(IV)–GLU, Colàs et al. (2011) reported a significant decrease in $[GLU]_{tot}$ due to its sorption on the actinide solid phase. Note however that the decrease in gluconate concentration observed by these authors occurred in a system with a larger amount of solid phase (3 g/L $Th(OH)_4$(am), compared to 250 mg/L – 500 mg/L $Nd(OH)_3$(s) in this study), and with an amorphous solid phase with an expectedly larger surface area.

Fig. 5 shows the X-ray diffractograms of the solid phases collected from solubility experiments in 0.1 M NaCl and 0.25 M $CaCl_2$ solutions. The figure includes also the diffractogram of the starting material Nd$(OH)_3$(s), which is in excellent agreement with the Nd$(OH)_3$(cr) reference in the JCPDS database (Wong-Ng et al., 2001). These XRD data confirm the presence of Nd$(OH)_3$(s) in the investigated samples, and disregard the presence of any additional (crystalline) Nd(III) secondary phase under the conditions of the experiments.

The possible formation of a ternary Ca–Nd(III)–GLU solid phase was proposed in Section 3.1 as a hypothesis to explain the observed solubility of Nd(III) at high gluconate concentrations. This hypothesis is not confirmed by XRD data discussed in this section, which however cannot disregard the co-existence of an amorphous Ca–Nd(III)–GLU solid phase or surface layer controlling the solubility of Nd(III) under these conditions. In a recent study, Böszörményi and co-workers studied the formation of Nd(III) solid phases in the binary Nd(III)–GLU and ternary Ca–Nd(III)–GLU systems (Böszörményi et al., 2020). The authors

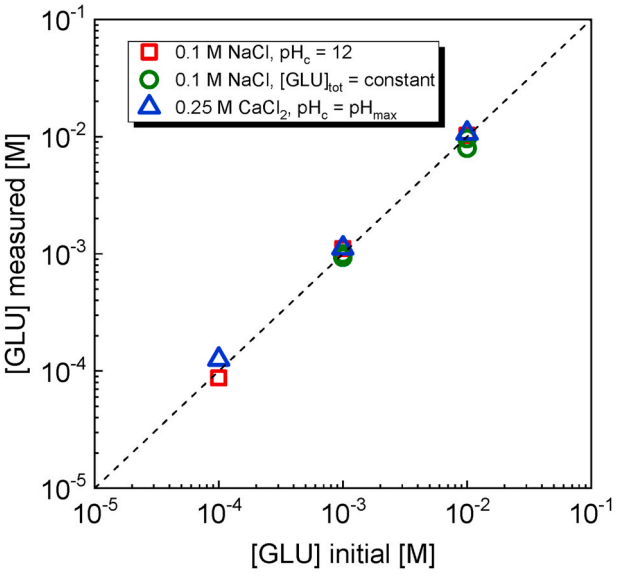

Fig. 4. Comparison of initially dissolved gluconate concentration with $[GLU]_{tot}$ experimentally determined by TOC after equilibration with Nd$(OH)_3$(s) in 0.1 M NaCl and 0.25 M $CaCl_2$ solutions. Series 0.1 M NaCl, pH_c = constant ≈12: $[GLU]_{ini}$ = 10^{-2}, 10^{-3} and 10^{-4} M. Series 0.1 M NaCl, $[GLU]_{tot}$ = constant: $[GLU]_{ini}$ = 10^{-3} M, pH_c = 8.48, 9.80, 10.89, 11.87, 12.34, 12.86; $[GLU]_{ini}$ = 10^{-2} M, pH_c = 10.86. Series 0.25 M $CaCl_2$, pH_c = constant = pH_{max}: $[GLU]_{ini}$ = 10^{-2} M, pH_c = 12.01; $[GLU]_{ini}$ = 10^{-3} M, pH_c = 12.17, $[GLU]_{ini}$ = 10^{-4} M, pH_c = 12.15.

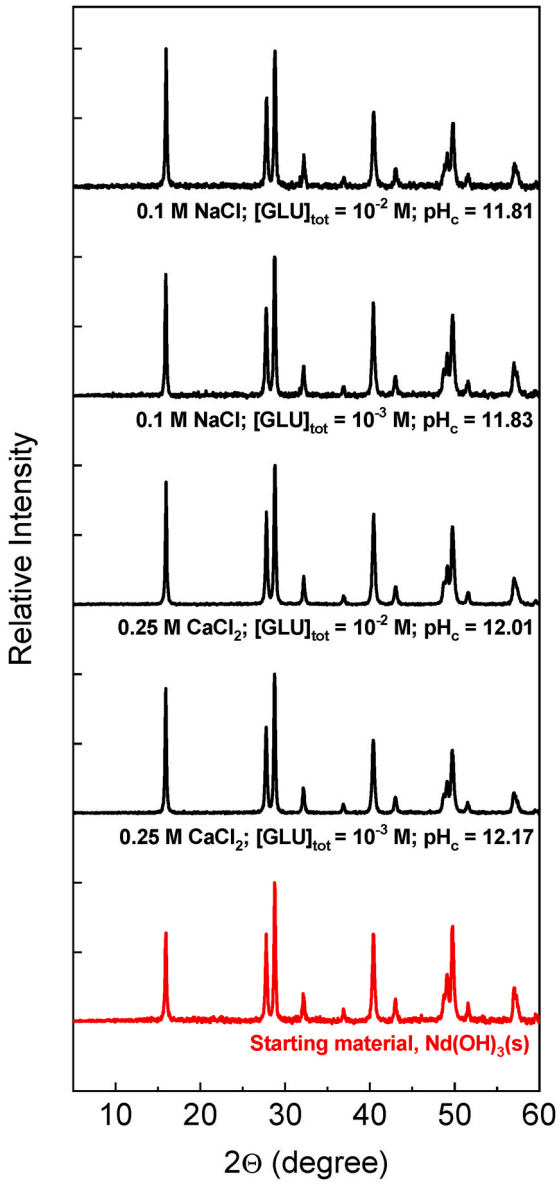

Fig. 5. X-ray diffractograms of solid phases recovered from selected Nd(III) solubility samples equilibrated in 0.1 M NaCl and 0.25 M $CaCl_2$ solutions in the presence of gluconate ($[GLU]_{tot}$ = 10^{-3} – 10^{-2} M). Diffractogram of the starting material Nd$(OH)_3$(s) used for the preparation of the solubility samples is included for comparison purposes.

investigated this system in largely oversaturated solutions (with ca. 0.1 M Nd(III)), and reported the formation of $CaNdGLU_{-H}(OH)_3{\cdot}4H_2O$(cr)[2] at pH ≈ 12. Although acknowledging the significantly different preparation methods, an analogous (amorphous) solid phase may have formed in the conditions of our experiments.

3.3. Cm(III) TRLFS in NaCl and $CaCl_2$ solutions in the presence of GLU

Cm(III) TRLFS studies focused on hyperalkaline pH conditions, *i.e.* pH_c ≈ 12, for which solubility data confirmed the greatest effect of gluconate (see Figs. 2 and 3). Fig. 6 shows the Cm(III) TRLFS spectra collected in 0.1 M NaCl solutions with 10^{-6} M ≤ $[GLU]_{tot}$ ≤ 1.1 × 10^{-3} M at three different Ca concentrations: (a, b) no Ca, (c, d) $[Ca]_{tot}$ = 10^{-3}

[2] "GLU_{-H}" corresponds to a gluconate molecule in which one of the alcohol groups is deprotonated.

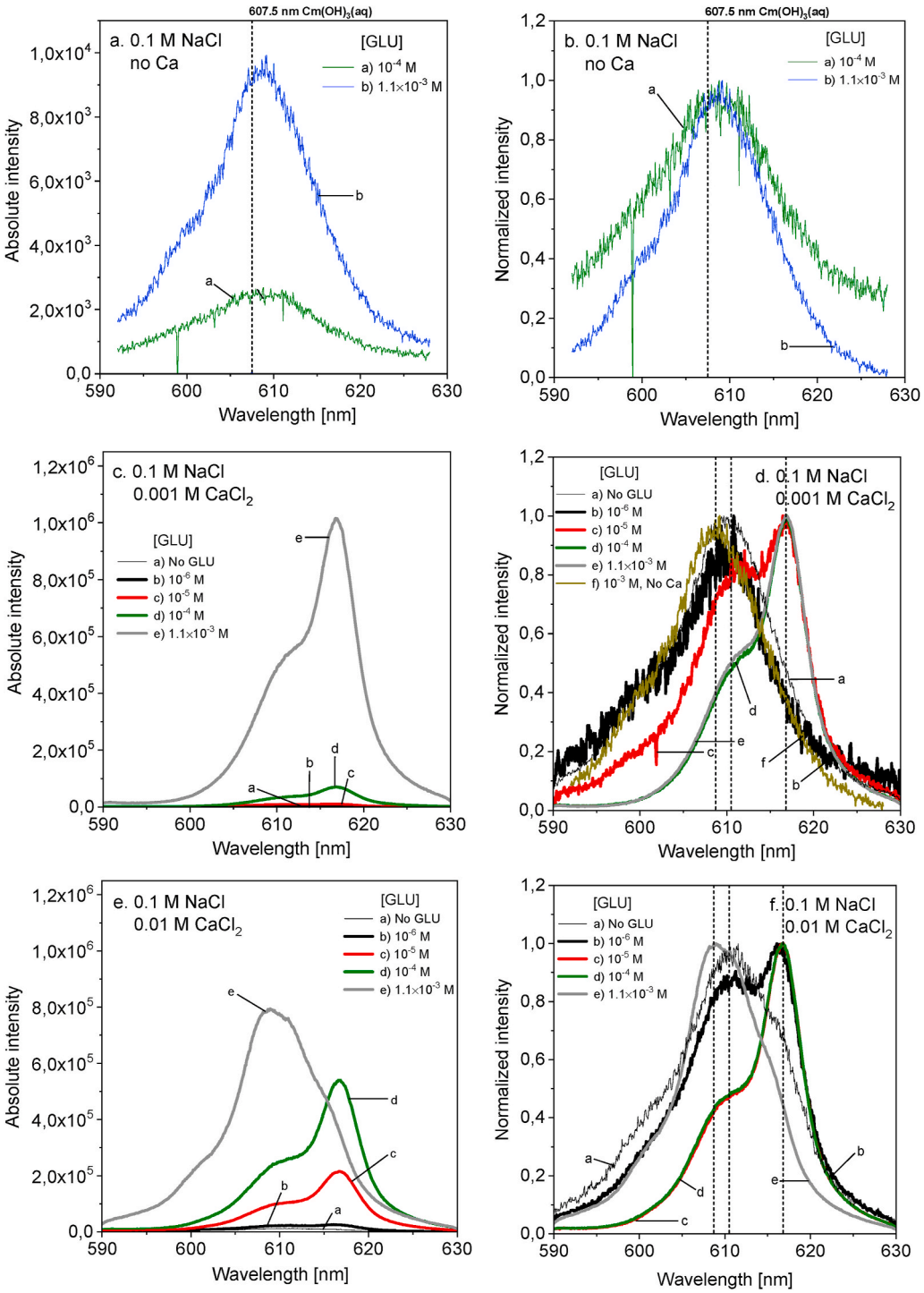

Fig. 6. TRLFS emission spectra of Cm(III) (absolute and peak height normalized intensities) in 0.1 M NaCl solutions at $pH_c \approx 12$ and $0 \leq [GLU]_{tot} \leq 1.1 \times 10^{-3}$ M. Test solutions investigated at three different calcium concentrations: (a, b) no Ca; (c, d) $[Ca]_{tot} = 10^{-3}$ M; (e, f) $[Ca]_{tot} = 10^{-2}$ M. See text for explanation of the dotted lines.

M and (e, f) $[Ca]_{tot} = 10^{-2}$ M. Fig. 7 summarizes the Cm(III) TRLFS spectra collected in $CaCl_2$ solutions with 10^{-6} M $\leq [GLU]_{tot} \leq 3.2 \times 10^{-3}$ M: (a, b) 0.1 M $CaCl_2$; (c, d) 0.25 M $CaCl_2$ and (e, f) 3.5 M $CaCl_2$. Figs. SI-1 and SI-2 in the Supporting Information (SI) document provide a more extensive TRLFS spectra dataset.

Fig. 6a and b shows less intense fluorescence signals for the binary system Cm(III)–GLU in 0.1 M NaCl solutions indicating sorption and/or precipitation of Cm(III) occurring under these conditions (initial Cm(III) concentration: 10^{-7} M; oversaturated according to Fig. 2a). The fluorescence intensity increase with increasing GLU concentrations points to a reduced sorption/precipitation of Cm(III) in the presence of higher GLU concentrations and/or to a (weak) aqueous complexation with GLU. Considering the scattered normalized spectra in Fig. 6b no significant difference in the fluorescence peak positions can be deduced. The dashed line included in both figures at $\lambda \approx 607.5$ nm corresponds to the peak position of $Cm(OH)_3(aq)$, the aqueous Cm(III) hydrolysis species expected to prevail in GLU-free solutions of analogous pH_c and salt concentration (Altmaier et al., 2009; Rabung et al., 2008). The only

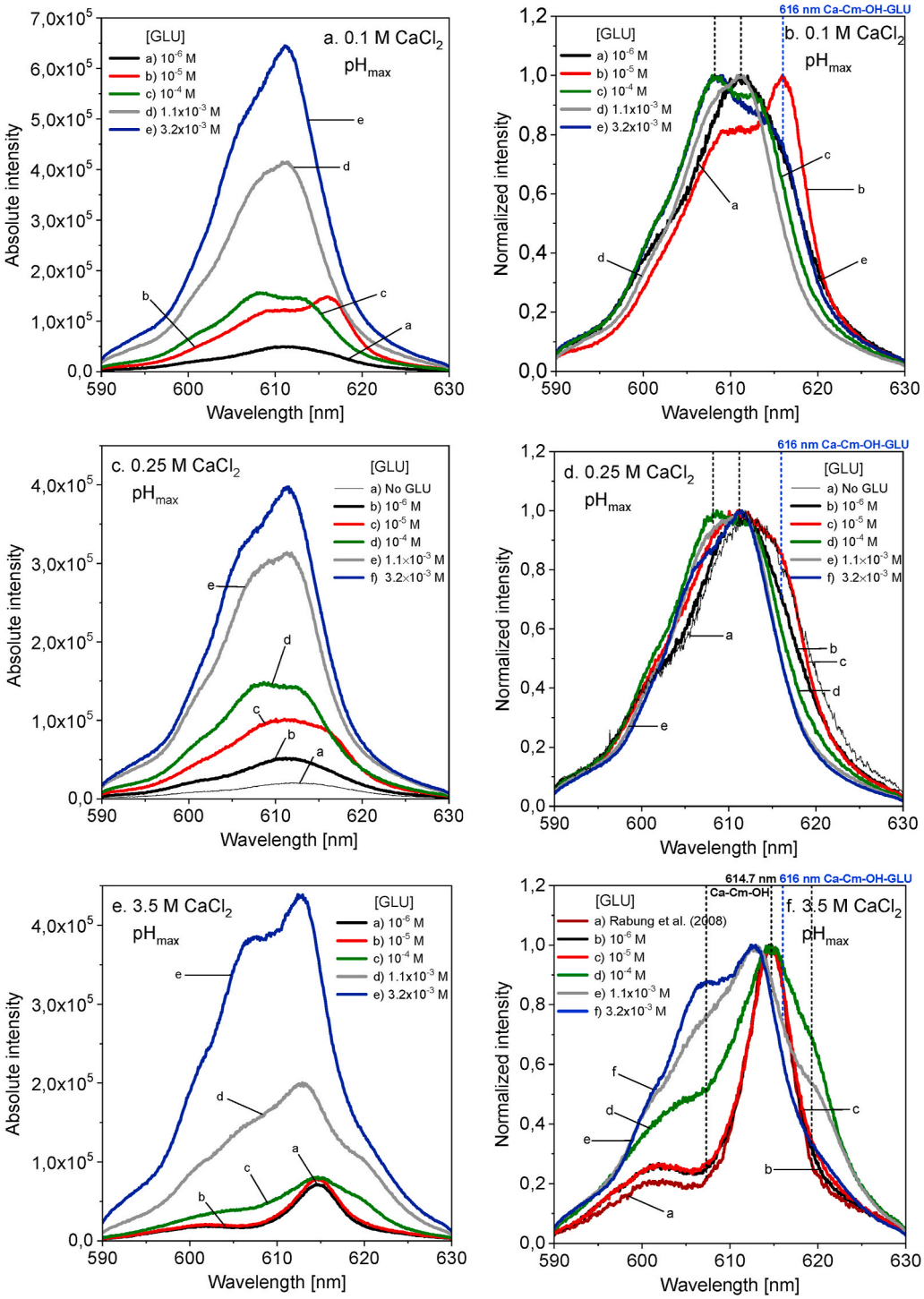

Fig. 7. TRLFS emission spectra of Cm(III) (absolute and height normalized intensities) in $CaCl_2$ solutions at $pH_c \approx 12$ and $0 \leq [GLU]_{tot} \leq 3.2 \times 10^{-3}$ M. Test solutions investigated at three different calcium concentrations: (a, b) $[CaCl_2] = 0.1$ M; (c, d) $[CaCl_2] = 0.25$ M; (e, f) $[CaCl_2] = 3.5$ M. See text for explanation of the dotted lines.

band observed in the investigated conditions (10^{-6} M $\leq [GLU]_{tot} \leq 1.1 \times 10^{-3}$ M) arises at $\lambda \approx 610$ nm. In a previous TRLFS study investigating the hydrolysis of Cm(III) in NaCl and $CaCl_2$ systems, Rabung et al. (2008) assigned the band at $\lambda = 609.9$ nm to the moiety "$Cm(OH)_4^-$" (either with or without Ca in the third coordination sphere). Considering the very similar wavelengths observed for both species, an aqueous complex of the type "$Cm(OH)_3GLU^-$" can be speculated to form in the Ca-free gluconate system. On the basis of their sorption data, Tits et al. (2005) reported the formation of the complex $EuGLU^-_{-3H}$ at pH = constant = 13.3. This complex formally holds the same stoichiometry as $Eu(OH)_3GLU^-$, but involves the deprotonation of three alcohol groups of gluconate instead of the hydrolysis of the Eu^{3+} cation. To our understanding, additional experimental efforts are required to provide definitive insights on the stoichiometry of the Ln(III)/An(III)–GLU complexes forming in hyperalkaline pH systems and absence of Ca. Note also that in spite of the clear evidence on Cm(III)–GLU complexation provided by TRLFS at $[GLU]_{tot} \geq 10^{-4}$ M (Fig. 6b), the solubility of Nd (III) in NaCl solutions and absence of Ca remained unaffected at

$[GLU]_{tot} = 10^{-3}$ M (Fig. 2a). As discussed in previous studies, these results highlight the sensitivity of TRLFS technique to investigate the speciation of Cm(III) at very low metal concentrations (Edelstein et al., 2006; Rabung et al., 2008).

The addition of Ca to the 0.1 M NaCl systems induces significant changes in the Cm(III) TRLFS spectra (Fig. 6c–f). Fluorescence intensity is importantly increased, whereas the wavelength of the main band experiences a very large red shift to $\lambda \approx 617$ nm (generally, an increased red shift points to a higher number of coordinating ligands or coordination with "stronger" ligands). Both observations are consistent with the formation of a strong complex, most likely involving a chelate-like structure that justifies the shift of ≈7 nm with respect to the Ca-free system. We note here that, in the context of a solubility study on the system Ca–Pu–OH–ISA, Tasi and co-workers reported the formation of the complex $CaPu^{IV}(OH)_3ISA_{-2H}(aq)$ in Tasi et al. (2018a). Based on DFT calculations, the authors were able to report the formation of a strong chelate complex involving the deprotonation of two alcohol groups of the ISA molecule.

A blue-shift (with respect to the 617 nm peak) is observed in the Cm (III) TRLFS spectra collected in 0.1 M NaCl solutions with 0.01 M $CaCl_2$ when $[GLU]_{tot} \geq 7 \times 10^{-4}$ M (see Figure SI-1), leading to the formation of two bands at $\lambda \approx 608$ nm and $\lambda \approx 611$ nm. A similar trend (with analogous bands at $\lambda \approx 608$ nm and $\lambda \approx 611$ nm) is observed in all Cm (III) spectra collected in 0.1 M and 0.25 M $CaCl_2$ solutions (both series are quite similar in respect to spectral properties), thus confirming the key role of Ca in the formation of such complexes (Fig. 7a–d). The unexpected blue shift might be related to the weakening of the original chelate complex in favour of a complex involving the incorporation of a second gluconate ligand to the coordination sphere of Cm(III). Additional discussion in this respect is provided in Section 3.4 on the basis of DFT calculations for the system Ca–Nd(III)–GLU.

Fig. 7e and f shows the impact of increasing gluconate concentrations on the Cm(III) TRLFS spectra collected in 3.5 M $CaCl_2$ solutions at $pH_c = pH_{max}$. A very significant red-shift with peak maxima at $\lambda = 614.7$ nm is observed at low gluconate concentrations ($[GLU]_{tot} < 10^{-4}$ M, compared to Ca-free systems and dilute $CaCl_2$ solutions. The peak position and peak shape are in excellent agreement with those of Cm(III) TRLFS spectra reported by Rabung et al. (2008) in GLU-free solutions of analogous composition. Combining solubility and TRLFS data, these authors assigned this band to the aqueous complex $Ca_3[Cm(OH)_6]^{3+}$, which is possibly also predominating under the conditions of our study (at low gluconate concentrations). A peak broadening (with shoulders at $\lambda \approx 607$ nm and ≈619 nm) is observed at higher gluconate concentrations, possibly corresponding to the formation of yet undefined Ca–Cm (III)–GLU complexes. However, as in the case of NaCl solutions, these spectroscopic observations do not translate into a clear impact on the solubility of Nd(III) under the same boundary conditions (see Fig. 2d). From the combined solubility and TRLFS experimental results obtained in the present work, it appears evident that binary Ca–GLU complexes forming in concentrated $CaCl_2$ solutions effectively outcompete the complexation of gluconate with Ln(III)/An(III).

3.4. Aqueous speciation of the ternary system Ca–An(III)/Ln(III)–GLU: additional insights from thermodynamic and DFT calculations

Solubility data discussed in Section 3.1 supports the formation of ternary complexes Ca–Nd(III)–GLU in dilute $CaCl_2$ solutions with pH_c above ≈ 11. Slope analyses in Fig. 2 (log [Nd(III)] *vs.* pH_c) and Fig. 3 (log [Nd(III)] *vs.* log $[GLU]_{tot}$) suggests the possible formation of a complex with stoichiometry Nd : OH = 1 : 6 or 7[3] and Nd : GLU = 1 : 2.

Cm(III) TRLFS data summarized in Section 3.3 provides unequivocal evidence on the formation of ternary complexes Ca–Cm(III)–GLU, although showing a far more complex aqueous speciation than described by solubility data. Up to five different features (either as main bands or shoulders, *i.e.* $\lambda \approx 607$, 608, 611, 616 and 619 nm) can be related to ternary Ca–Cm(III)–GLU interactions. We note, however, that some/most of these bands may not correspond to predominant species in solution, and thus have only a minor impact in the solubility data.

Additional insight on the aqueous speciation of the ternary system Ca–An(III)/Ln(III)–GLU can be gained by considering the predominant species in the corresponding binary systems Ca–An(III)/Ln(III) and Ca–GLU under the investigated boundary conditions. Fig. 8 shows the fraction diagrams of Nd(III) and GLU in 0.01, 0.1 and 0.25 M $CaCl_2$ solutions, as calculated using thermodynamic data reported by Neck et al. (2009) (Nd(III) system) and Pallagi et al. (2014) (GLU system).

Fig. 8a–c show that, in the absence of gluconate, $Nd(OH)_3(aq)$ is the main Nd(III) species in 0.01–0.25 M $CaCl_2$ solutions with $pH_c \geq 11$. Only in 0.25 M $CaCl_2$ solutions with $pH_c \approx 12$, the ternary species $Ca_2[Nd(OH)_4]^{3+}$ and $Ca_3[Nd(OH)_6]^{3+}$ prevail. The complexes GLU^- and $CaGLU^+$ control the solution chemistry of gluconate in 0.01–0.25 M $CaCl_2$ solutions with pH_c below ≈11.3. Above this pH_c, the complex $Ca_3(OH)_4GLU_2(aq)$ becomes the predominant gluconate species in solution. We note that the formal description of this complex likely involves the deprotonation of two alcohol groups of gluconate, *i.e.* $Ca_3(GLU_{-2H})_2(aq)$, instead of the four hydroxide groups proposed by Pallagi and co-workers (Pallagi et al., 2014). The overall stoichiometry of the complexation reaction is the same in both formulations.

The complexity of the aqueous speciation in the ternary system Ca–An(III)/Ln(III)–GLU as highlighted by TRLFS is further supported by thermodynamic calculations for the two binary systems Ca–An(III)/Ln (III) and Ca–GLU (Fig. 8). A rough approach to explore qualitatively the complexes forming in the ternary system considers the combination of the predominant complexes in the corresponding binary systems at $pH_c \geq 11.5$:

$$Nd(OH)_3(aq) + Ca_3(OH)_4GLU_2(aq) \Leftrightarrow Ca_3Nd(OH)_7GLU_2(aq) \quad (1)$$

The moiety "$Nd(OH)_7GLU_2^{6-}$" is consistent with the tentative slope analyses discussed in Section 3.2. Our results do not provide experimental evidence on the number of Ca-atoms participating in the ternary complex Ca–An(III)/Ln(III)–GLU. Although the formation of a neutral complex in the presence of a large excess of Ca^{2+} (as occurring in 0.1 and 0.25 M $CaCl_2$) appears reasonable,[4] further experimental results are required to validate this hypothesis.

Fig. 8 shows also that the species $Ca_2(OH)_3GLU(aq)$ gains relevance with increasing Ca concentration, and accordingly is expected to become predominant in concentrated $CaCl_2$ solutions. Data collected for the system Nd(III)–GLU in 3.5 M $CaCl_2$ show no impact of GLU on the solubility compared to GLU-free systems, which indicates that binary Ca–GLU complexes outcompete the formation of the ternary complexes Ca–An(III)/Ln(III)–GLU. Note that the latter aspect can be only fulfilled when the ratio Ca : GLU in the binary complex Ca–GLU is greater than in the ternary complex Ca–An(III)/Ln(III)–GLU.

Due to the uncertainties affecting to the stoichiometry of the ternary Ca–An(III)/Ln(III)–GLU complexes, DFT calculations conducted in this

[3] The slope of the solubility data in 0.25 M $CaCl_2$ at $pH_c \geq 11$ is + 3/+4, indicating that 3–4 H^+ are released in the chemical equilibrium controlling the solubility in these conditions. Considering that the solid phase controlling the solubility is $Nd(OH)_3(s)$, the ratio Nd : OH in the complex predominating in the aqueous phase is 1 : (3 + 3) or 1 : (3 + 4).

[4] Ternary complexes involving the participation of 1 and 2 Ca-atoms result in negatively charged complexes, $CaNd(OH)_7GLU_2^{4-}$ and $Ca_2Nd(OH)_7GLU_2^{2-}$, which are expected to strongly interact with calcium in the presence of a large excess of Ca^{2+}.

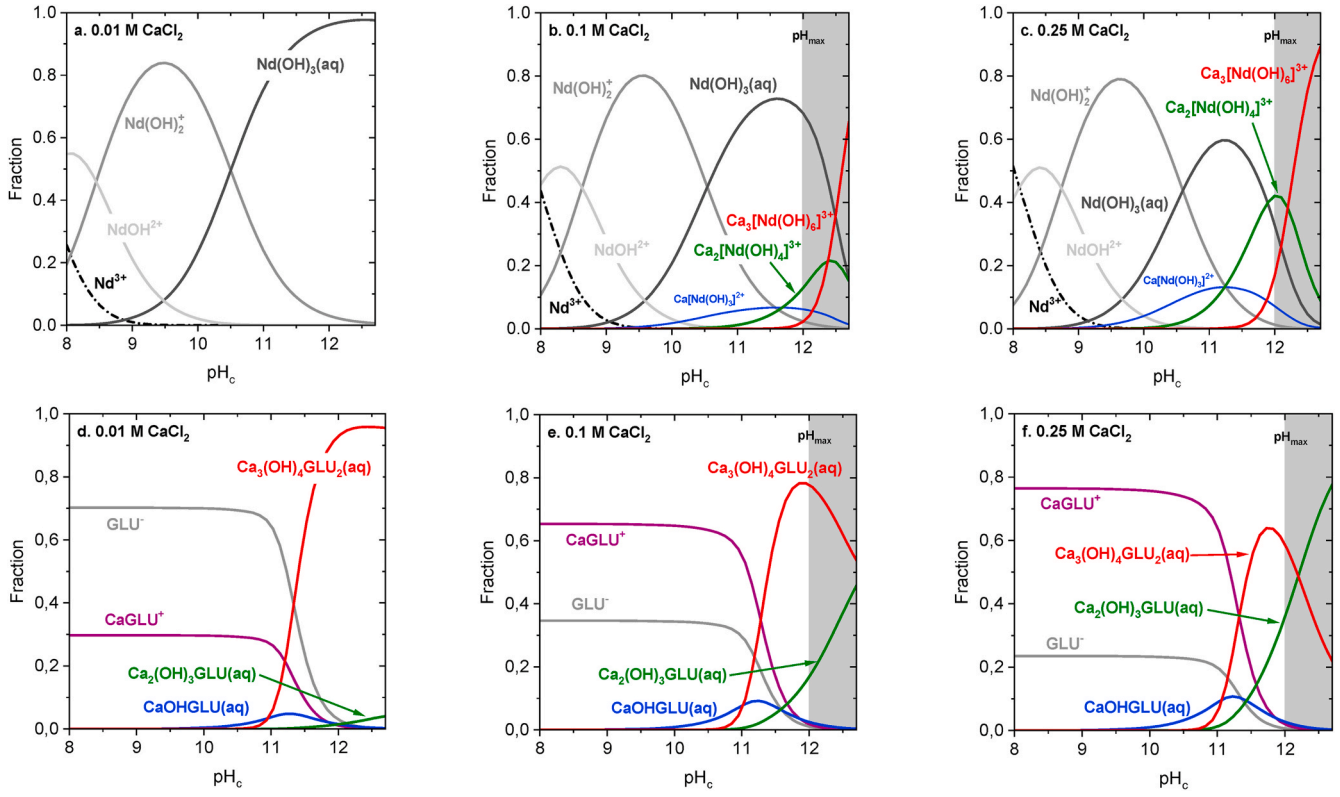

Fig. 8. Fraction diagrams of Nd(III) calculated for (a) 0.01 M $CaCl_2$; (b) 0.1 M $CaCl_2$; (c) 0.25 M $CaCl_2$ using thermodynamic data reported in Neck et al. (2009). Fraction diagrams of gluconate calculated for $[GLU]_{tot} = 10^{-3}$ M and (d) 0.01 M $CaCl_2$; (e) 0.1 M $CaCl_2$; (f) 0.25 M $CaCl_2$ using thermodynamic data reported in Pallagi et al. (2014). pH_c in 0.1 and 0.25 M $CaCl_2$ systems buffered to $pH_{max} \approx 12$ due to the precipitation of $Ca(OH)_2$ (shadowed region in figures b, c, e and f).

work exemplarily targeted the neutral complex described above, *i.e.* $Ca_3Nd(OH)_7GLU_2(aq)$. These calculations probed the deprotonation of H_2O in the vicinity of Nd (*i.e.* hydrolysis of neodymium) *vs.* the deprotonation of alcohol groups in the gluconate molecule. The structures of four different complexes ($Ca_3Nd(OH)_7GLU_2(aq)$, $Ca_3Nd(OH)_5(GLU_{-H})_2(aq)$, $Ca_3Nd(OH)_3(GLU_{-2H})_2(aq)$ and $Ca_3NdOH(GLU_{-3H})_2(aq)$) were optimized by DFT considering explicitly the presence of a number of water molecules to find out the energetically most likely deprotonation scheme. Furthermore, COSMO was considered to account for additional solvent effects in the system.

Our DFT calculations show that the lowest energy is found for the complex with both gluconates equally deprotonated and one hydroxide group present in the vicinity of Nd, $Ca_3NdOH(GLU_{-3H})_2(aq)$ (Fig. 9). The average Nd–O distances in this complex are (251.1 ± 3.6) and (251.5 ± 3.8) pm, as calculated respectively without and with the use of the COSMO solvation model (Table 1). The shortest Nd–O distances are obtained for the deprotonated alcohol groups of GLU, whereas the longest distances are calculated for the deprotonated carboxylate groups of GLU. This result highlights the key role of the alcohol groups of gluconate in the complex formation with hard-Lewis acids such as Nd (III). The distances calculated for Nd-OH^- and Nd-OH_2 lay in between those obtained for alcohol and carboxylate groups belonging to gluconate.

Additional calculations with only two or one Ca^{2+} ions in the complex showed that these, now highly charged moieties, are stable as well. Due to the high charges and related computational challenges, we do not give any qualitative results for these two latter complexes.

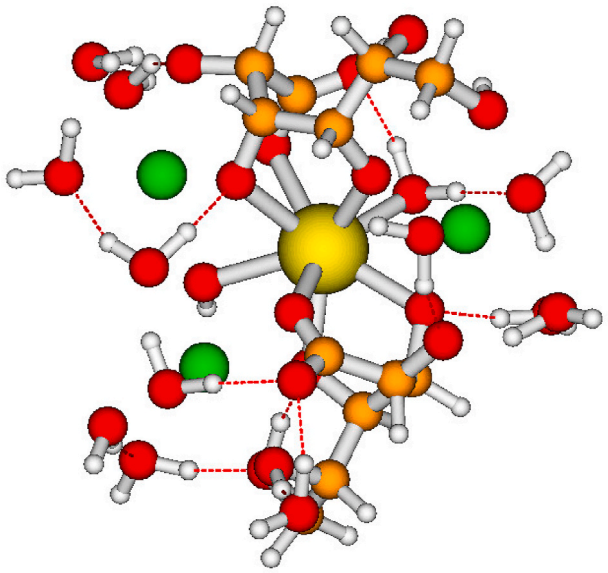

Fig. 9. Structure of the ternary complex $Ca_3NdOH(GLU_{-3H})_2(aq)$ as optimized by DFT calculations. Colour code: Nd: yellow; Ca: green; O: red; C: orange; H: grey.

4. Conclusions

The complexation of gluconate with Ln(III) and An(III) in alkaline NaCl and $CaCl_2$ solutions was systematically investigated by a combination of solubility, spectroscopic and theoretical methods. Focus is given to evaluate the possible formation of ternary complexes with calcium and their impact on the solubility of Ln(III) and An(III).

The solubility of Nd(III) in the presence of gluconate at $[GLU]_{tot} = 10^{-3}$ M and in the absence of calcium remains unaffected in alkaline NaCl solutions, although TRLFS confirms the formation of a binary Cm

Table 1
Nd–O distances for $Ca_3NdOH(GLU_{-3H})_2$ calculated with DFT(BP86/def2-SVP) and DFT(BP86/def2-SVP)+COSMO (all distances in pm).

	DFT(BP86/def2-SVP)		DFT(BP86/def2-SVP)+COSMO
Nd-GLU(O^-)	234.1	Nd-GLU(O^-)	235.1
Nd-GLU(O^-)	242.9	Nd-GLU(O^-)	243.4
Nd-GLU(O^-)	243.5	Nd-GLU(O^-)	243.8
Nd-OH_2	253.2	Nd-GLU(O^-)	251.2
Nd-GLU(O^-)	253.8	Nd-OH^-	252.8
Nd-OH^-	256.6	Nd-OH_2	257.0
Nd-GLU(COO^-)	258.6	Nd-GLU(COO^-)	259.0
Nd-GLU(COO^-)	265.7	Nd-GLU(COO^-)	269.9
Ca-GLU(O^-)	234.7	Ca-GLU(O^-)	236.4
Ca-GLU(O^-)	247.7	Ca-GLU(O^-)	248.8

(III)–GLU complex with peak maximum at $\lambda \approx 607$ nm. In dilute $CaCl_2$ solutions (0.1 and 0.25 M) with $pH_c \geq 11$, gluconate significantly enhances the solubility of Nd(III) at $[GLU]_{tot} \geq 10^{-4}$ M. These observations strongly hint towards the formation and predominance of ternary Ca–Nd(III)–GLU complexes in the aqueous phase. The comparison of TRLFS collected for the Cm(III)–GLU systems in the absence and presence of Ca provides additional evidence on the formation of ternary complexes Ca–Cm(III)–GLU complexes. Up to five fluorescence bands or shoulders (at $\lambda \approx 607$, 608, 611, 616 and 620 nm) are associated to ternary Ca–Cm(III)–GLU interactions, although some of these bands may not correspond to predominant species in solution. DFT calculations further support the stability of ternary Ca–Nd(III)–GLU complexes, which involve the deprotonation of up to three alcohol groups of the gluconate molecule.

As indicated by solubility and TRLFS experiments, binary complexes Ca–GLU forming in concentrated $CaCl_2$ solutions effectively outcompete the complexation of Ln(III) and An(III) with gluconate. This observation supports the formation of binary Ca–GLU complexes with a greater Ca : GLU ratio than in the ternary Ca–Ln(III)/An(III)–GLU complexes.

This work provides an important contribution to understand the impact of gluconate on the solution chemistry of Ln(III) and An(III) under repository relevant conditions. Experimental results and theoretical calculations obtained in this work underpin the very complex aqueous speciation of Ln(III) and An(III) in the presence of gluconate and calcium, and provide tools to assess upper concentration limits of trivalent actinides that can be used for source term estimations. Comprehensive thermodynamic and activity models will be presented separately based on systematic solubility experiments with Nd(III) in dilute to concentrated NaCl and $CaCl_2$ systems under varying gluconate concentrations.

Declaration of competing interest

The authors declare that they have no known competing financial interests or personal relationships that could have appeared to influence the work reported in this paper.

Acknowledgements

F. Geyer (KIT–INE) is kindly acknowledged for conducting the ICP–MS measurements. H. Rojo acknowledges ACTINET–i3 Integrated Infrastructure Initiative for financial support. This work was partly funded by the German Ministry of Economic Affairs and Energy (BMWi) within the framework of the GRAZ project under the contract number 02E11415C.

Appendix A. Supplementary data

Supplementary data to this article can be found online at https://doi.org/10.1016/j.apgeochem.2020.104864.

References

Ahlrichs, R., Furche, F., Grimme, S., Cohen, A.J., Handy, N.C., 2000. Comment on "Assessment of exchange correlation functionals. Chem. Phys. Lett. 316 (2000), 160–166. Chemical Physics Letters 325, 317-321.
Allard, S., 2005. Investigations of α-D-isosaccharinate: Fundamental Properties and complexation., Doktorsavhandlingar Vid Chalmers Tekniska Hogskola. Chalmers University of Technology, Sweden.
Allard, S., Ekberg, C., 2006. Complexing properties of alpha-isosaccharinate: stability constants, enthalpies and entropies of Th-complexation with uncertainty analysis. J. Solut. Chem. 35, 1173–1186.
Altmaier, M., Gaona, X., Fanghänel, T., 2013. Recent advances in aqueous actinide chemistry and thermodynamics. Chem. Rev. 113, 901–943.
Altmaier, M., Metz, V., Neck, V., Müller, R., Fanghänel, T., 2003. Solid-liquid equilibria of $Mg(OH)_2$(cr) and $Mg_2(OH)_3Cl{\cdot}4H_2O$(cr) in the system Mg-Na-H-OH-O-Cl-H_2O at 25°C. Geochem. Cosmochim. Acta 67, 3595–3601.
Altmaier, M., Neck, V., Fanghanel, T., 2008. Solubility of Zr(IV), Th(IV) and Pu(IV) hydrous oxides in $CaCl_2$ solutions and the formation of ternary Ca-M(IV)-OH complexes. Radiochim. Acta 96, 541–550.
Altmaier, M., Neck, V., Lützenkirchen, J., Fanghänel, T., 2009. Solubility of plutonium in $MgCl_2$ and $CaCl_2$ solutions in contact with metallic iron. Radiochim. Acta 97, 187–192.
Bechtold, T., Burtscher, E., Turcanu, A., 2002. Ca^{2+}-Fe^{3+}-D-gluconate-complexes in alkaline solution. Complex stabilities and electrochemical properties. Dalton Trans. 13, 2683–2688.
Berner, U.R., 1992. Evolution of pore water chemistry during degradation of cement in a radioactive waste repository environment. Waste Manag. 12, 201–219.
Böszörményi, É., Lado, J., Dudás, C., Kutus, B., Szabados, M., Varga, G., Pálinkó, I., Sipos, P., 2020. The structure and composition of solid complexes comprising of Nd(III), Ca(II) and D-gluconate isolated from solutions relevant to radioactive waste disposal. Pure Appl. Chem. 92, 1709–1715.
Brewitz, W., 1980. Zusammenfassender Zwischenbericht, GSF T 114. Ges. f. Strahlen- und Umweltforschung, Braunschweig.
Bube, C., Metz, V., Bohnert, E., Garbev, K., Schild, D., Kienzler, B., 2013. Long-term cement corrosion in chloride-rich solutions relevant to radioactive waste disposal in rock salt - leaching experiments and thermodynamic simulations. Phys. Chem. Earth 64, 87–94.
Colàs, E., 2014. Complexation of Th(IV) and U(VI) by Polyhydroxy and Polyamino Carboxylic Acids. PhD thesis. Departament d'Enginyeria Química Universitat Politecnica de Catalunya, Spain.
Colàs, E., Grivé, M., Rojo, I., 2013a. Complexation of uranium(VI) by gluconate in alkaline solutions. J. Solut. Chem. 42, 1545–1557.
Colàs, E., Grivé, M., Rojo, I., Duro, L., 2011. Solubility of $ThO_2{\cdot}xH_2O$(am) in the presence of gluconate. Radiochim. Acta 99, 269–273.
Colàs, E., Grivé, M., Rojo, I., Duro, L., 2013b. The effect of gluconate and EDTA on thorium solubility under simulated cement porewater conditions. J. Solut. Chem. 42, 1680–1690.
Deglmann, P., May, K., Furche, F., Ahlrichs, R., 2004. Nuclear second analytical derivative calculations using auxiliary basis set expansions. Chem. Phys. Lett. 384, 103–107.
Dolg, M., Stoll, H., Preuss, H., 1993. A combination of quasirelativistic pseudopotential and ligand field calculations for lanthanoid compounds. Theor. Chim. Acta 85, 441–450.
Dolg, M., Stoll, H., Savin, A., Preuss, H., 1989. Energy-adjusted pseudopotentials for the rare earth elements. Theor. Chim. Acta 75, 173–194.
Edelstein, N.M., Klenze, R., Fanghänel, T., Hubert, S., 2006. Optical properties of Cm(III) in crystals and solutions and their application to Cm(III) speciation. Coord. Chem. Rev. 250, 948–973.
Eichkorn, K., Treutler, O., Öhm, H., Häser, M., Ahlrichs, R., 1995. Auxiliary basis sets to approximate Coulomb potentials. Chem. Phys. Lett. 242, 652–660.
Eichkorn, K., Weigend, F., Treutler, O., Ahlrichs, R., 1997. Auxiliary basis sets for main row atoms and transition metals and their use to approximate Coulomb potentials. Theor. Chem. Acc. 97, 119–124.
Fellhauer, D., Altmaier, M., Gaona, X., Lützenkirchen, J., Fanghänel, T., 2016a. Np(V) solubility, speciation and solid phase formation in alkaline $CaCl_2$ solutions. Part II:

thermodynamics and implications for source term estimations of nuclear waste disposal. Radiochim. Acta 104, 381–397.
Fellhauer, D., Neck, V., Altmaier, M., Lützenkirchen, J., Fanghänel, T., 2010. Solubility of tetravalent actinides in alkaline $CaCl_2$ solutions and formation of $Ca_4[An(OH)_8]^{4+}$ complexes: a study of Np(IV) and Pu(IV) under reducing conditions and the systematic trend in the An(IV) series. Radiochim. Acta 98, 541–548.
Fellhauer, D., Rothe, J., Altmaier, M., Neck, V., Runke, J., Wiss, T., Fanghänel, T., 2016b. Np(V) solubility, speciation and solid phase formation in alkaline $CaCl_2$ solutions. Part I: experimental results. Radiochim. Acta 104, 355–379.
Furche, F., Ahlrichs, R., Hättig, C., Klopper, W., Sierka, M., Weigend, F., 2014. Turbomole. Wiley Interdiscipl. Rev.: Comput. Mol. Sci. 4, 91–100.
Gaona, X., Montoya, V., Colàs, E., Grivé, M., Duro, L., 2008. Review of the complexation of tetravalent actinides by ISA and gluconate under alkaline to hyperalkaline conditions. J. Contam. Hydrol. 102, 217–227.
Giroux, S., Rubini, P., Henry, B., Aury, S., 2000. Complexes of praseodymium(III) with D-gluconic acid. Polyhedron 19, 1567–1574.
Grenthe, I., Gaona, X., Plyasunov, A.V., Rao, L., Runde, W.H., Grambow, B., Konings, R.J. M., Smith, A.L., Moore, E.E., 2020. Chemical Thermodynamics. In: Second Update on the Chemical Thermodynamics of U, Np, Pu, Am and Tc. OECD Nuclear Energy Agency Data Bank, vol. 14. OECD Publications, Paris, France.
Guillaumont, R., Fanghänel, J., Neck, V., Fuger, J., Palmer, D.A., Grenthe, I., Rand, M.H., 2003. Chemical Thermodynamics Vol. 5. Update on the Chemical Thermodynamics of Uranium, Neptunium, Plutonium, Americium and Technetium. OECD Nuclear Energy Agency Data Bank. North Holland Elsevier Science Publishers B. V., Amsterdam, The Netherlands.
Hohenberg, P., Kohn, W., 1964. Inhomogeneous electron gas. Phys. Rev. 136, B864–B871.
Klamt, A., 1995. Conductor-like screening model for real solvents: a new approach to the quantitative calculation of solvation phenomena. J. Phys. Chem. 99, 2224–2235.
Klamt, A., Schüürmann, G., 1993. COSMO: a new approach to dielectric screening in solvents with explicit expressions for the screening energy and its gradient. J. Chem. Soc. Perkin Trans. 2, 799–805.
Kohn, W., Sham, L.J., 1965. Self-consistent equations including exchange and correlation effects. Phys. Rev. 140, A1133–A1138.
Kulik, D.A., 2011. Improving the structural consistency of C-S-H solid solution thermodynamic models. Cement Concr. Res. 41, 477–495.
Kutus, B., Gaona, X., Pallagi, A., Pálinkó, I., Altmaier, M., Sipos, P., 2020. Recent advances in the aqueous chemistry of the calcium(II)-gluconate system – equilibria, structure and composition of the complexes forming in neutral and in alkaline solutions. Coord. Chem. Rev. 417.
Moreton, A.D., 1993. Thermodynamic modeling of the effect of hydroxycarboxylic acids on the solubility of plutonium at high pH. Mater. Res. Soc. Symp. Proc. 294, 753–758.
Moreton, A.D., Pilkington, N.J., Tweed, C.J., 2000. Thermodynamic Modelling of the Effect of Hydroxycarboxylic Acids on the Solubility of Plutonium at High pH, UK NIREX Technical Report NSS/R339.
Motekaitis, R.J., Martell, A.E., 1984. Complexes of aluminum(III) with hydroxy carboxylic acids. Inorg. Chem. 23, 18–23.
Neck, V., Altmaier, M., Rabung, T., Lützenkirchen, J., Fanghänel, T., 2009. Thermodynamics of trivalent actinides and neodymium in NaCl, $MgCl_2$, and $CaCl_2$ solutions: solubility, hydrolysis, and ternary Ca-M(III)-OH complexes. Pure Appl. Chem. 81, 1555–1568.
Neck, V., Kim, J.I., 2001. Solubility and hydrolysis of tetravalent actinides. Radiochim. Acta 89, 1–16.
Pallagi, A., Bajnóczi, E.G., Canton, S.E., Bolin, T., Peintler, G., Kutus, B., Kele, Z., Pálinkó, I., Sipos, P., 2014. Multinuclear complex formation between Ca(II) and gluconate ions in hyperalkaline solutions. Environ. Sci. Technol. 48, 6604–6611.
Pallagi, A., Tasi, A.G., Peintler, G., Forgo, P., Palinko, I., Sipos, P., 2013. Complexation of Al(III) with gluconate in alkaline to hyperalkaline solutions: formation, stability and structure. Dalton Trans. 42, 13470–13476.
Rabung, T., Altmaier, M., Neck, V., Fanghänel, T., 2008. A TRLFS study of Cm(III) hydroxide complexes in alkaline $CaCl_2$ solutions. Radiochim. Acta 96, 551–559.
Rai, D., Hess, N.J., Xia, Y., Rao, L., Cho, H.M., Moore, R.C., Van Loon, L.R., 2003. Comprehensive thermodynamic model applicable to highly acidic to basic conditions for isosaccharinate reactions with Ca(II) and Np(IV). J. Solut. Chem. 32, 665–689.
Rai, D., Rao, L., Moore Dean, A., 1998. The influence of isosaccharinic acid on the solubility of Np(IV) hydrous oxide. Radiochim. Acta 83, 9–13.
Rai, D., Yui, M., Moore, D.A., Rao, L., 2009. Thermodynamic model for ThO_2(am) solubility in isosaccharinate solutions. J. Solut. Chem. 38, 1573–1587.
Rojo, H., Tits, J., Gaona, X., Garcia-Gutiérrez, M., Missana, T., Wieland, E., 2013. Thermodynamics of Np(IV) complexes with gluconic acid under alkaline conditions: sorption studies. Radiochim. Acta 101, 133–138.
Schäfer, A., Horn, H., Ahlrichs, R., 1992. Fully optimized contracted Gaussian basis sets for atoms Li to Kr. J. Chem. Phys. 97, 2571–2577.
Tasi, A., Gaona, X., Fellhauer, D., Böttle, M., Rothe, J., Dardenne, K., Polly, R., Grivé, M., Colàs, E., Bruno, J., Källstrom, K., Altmaier, M., Geckeis, H., 2018a. Thermodynamic description of the plutonium – α–D–isosaccharinic acid system ii: formation of quaternary Ca(II)–Pu(IV)–OH–ISA complexes. Appl. Geochem. 98, 351–366.
Tasi, A., Gaona, X., Fellhauer, D., Böttle, M., Rothe, J., Dardenne, K., Polly, R., Grivé, M., Colàs, E., Bruno, J., Källström, K., Altmaier, M., Geckeis, H., 2018b. Thermodynamic description of the plutonium – α–D–isosaccharinic acid system I: solubility, complexation and redox behavior. Appl. Geochem. 98, 247–264.
Tits, J., Wieland, E., Bradbury, M.H., 2005. The effect of isosaccharinic acid and gluconic acid on the retention of Eu(III), Am(III) and Th(IV) by calcite. Appl. Geochem. 20, 2082–2096.
Treutler, O., Ahlrichs, R., 1995. Efficient molecular numerical integration schemes. J. Chem. Phys. 102, 346–354.
Vercammen, K., 2000. Complexation of Calcium, Thorium and Europium by α-isosaccharinic Acid under Alkaline Conditions. Swiss Federal Institute of Technology, Switzerland.
Vercammen, K., Glaus, M.A., Van Loon, L.R., 1999. Evidence for the existence of complexes between Th(IV) and alpha-isosaccharinic acid under alkaline conditions. Radiochim. Acta 84, 221–224.
Vercammen, K., Glaus, M.A., Van Loon, L.R., 2001. Complexation of Th(IV) and Eu(III) by alpha-isosaccharinic acid under alkaline conditions. Radiochim. Acta 89, 393–401.
Von Arnim, M., Ahlrichs, R., 1999. Geometry optimization in generalized natural internal coordinates. J. Chem. Phys. 111, 9183–9190.
Wong-Ng, W., McMurdie, H.F., Hubbard, C.R., Mighell, A.D., 2001. JCPDS-ICDD research associateship (cooperative program with NBS/NIST). J. Res. Natl. Inst. Stand. Technol. 106, 1013–1028.
Yalçintaş, E., Gaona, X., Altmaier, M., Dardenne, K., Polly, R., Geckeis, H., 2016. Thermodynamic description of Tc(IV) solubility and hydrolysis in dilute to concentrated NaCl, $MgCl_2$ and $CaCl_2$ solutions. Dalton Trans. 45, 8916–8936.
Zhang, Z.C., Bottenus, B., Clark, S.B., Tian, G.X., Zanonato, P., Rao, L.F., 2007. Complexation of gluconic acid with Nd(III) in acidic solutions: a thermodynamic study. J. Alloys Compd. 444, 470–476.